

## Exciton-magnon splitting in the van der Waals antiferromagnet $\text{MnPS}_3$ unveiled by second-harmonic generation

Ziqian Wang <sup>1,\*</sup>,† Xiao-Xiao Zhang <sup>1,\*</sup>, Yuki Shiomi,<sup>2</sup> Taka-hisa Arima <sup>1,3</sup>,  
Naoto Nagaosa,<sup>1</sup> Yoshinori Tokura,<sup>1,4,5</sup> and Naoki Ogawa<sup>1</sup>

<sup>1</sup>*RIKEN Center for Emergent Matter Science (CEMS), Wako, Saitama 351-0198, Japan*

<sup>2</sup>*Department of Basic Science, University of Tokyo, Tokyo 153-8902, Japan*

<sup>3</sup>*Department of Advanced Materials Science, University of Tokyo, Kashiwa, Chiba 277-8561, Japan*

<sup>4</sup>*Department of Applied Physics, University of Tokyo, Tokyo 113-8656, Japan*

<sup>5</sup>*Tokyo College, University of Tokyo, Tokyo 113-8656, Japan*



(Received 17 September 2022; revised 1 September 2023; accepted 5 October 2023; published 30 November 2023)

Exciton-magnon pairwise excitation is promising to realize the direct and efficient photogeneration of magnons, especially in low-dimensional materials with large quasiparticle scattering cross sections. Using resonant second-harmonic generation spectroscopy, we identified exciton-magnon resonance in  $\text{MnPS}_3$  with possible splitting, in line with the exciton-induced modification of the magnon density of states based on our Koster-Slater-type theory. The substantial exciton-magnon interaction, favored by symmetry, sheds light on coherent cross control among charge, spin, and orbital degrees of freedom via quasiparticle correlations. Additionally, a large linear magnetoelectric effect of excitons is observed.

DOI: [10.1103/PhysRevResearch.5.L042032](https://doi.org/10.1103/PhysRevResearch.5.L042032)

Recent discoveries of two-dimensional (2D) van der Waals (vdW) antiferromagnets (AFMs)  $\text{MPX}_3$  ( $M = \text{Fe}, \text{Co}, \text{Ni}, \text{Mn}$ ;  $X = \text{S}, \text{Se}$ ) with intralayer antiferromagnetic orders have brought antiferromagnetic spintronics to an unprecedented 2D realm with significant correlation and quantum effects [1–4]. The Néel-type AFM  $\text{MnPS}_3$  hosts many attractive physical properties [5–9]. The reported linear magnetoelectric effect indicates the cross correlation of its electronic and magnetic systems [10]. Despite its potential as a superior 2D platform for magnon-based optospintronics, the efficient generation and control of magnons in  $\text{MnPS}_3$  via ultrafast optical means remains a central issue.

Magnons have been excited through the coupling between spin and intermediary excitations such as on-site  $d-d$  transitions in  $\text{MnPS}_3$  and Zhang-Rice excitons in  $\text{NiPS}_3$  [11–13]. However, such *indirect* excitation has less of a cross section and is typically confined to the Brillouin zone center, resulting in magnons with relatively low frequencies. On the other hand, the exciton fine structures in these vdW AFMs [4,14–17] manifest the fundamental role of quasiparticle correlations. In particular, the exciton-magnon coupling revealed by the magnon sideband in  $\text{MnPS}_3$  [17] suggests a possible route of ultrafast photogeneration of magnons carrying wave vectors throughout the Brillouin zone, by *direct* pairwise

photoexcitation of a magnon and a counterpropagating exciton. However, up to now, a fundamental understanding of the magnon properties under such pair excitation in vdW AFMs has been elusive.

Optical second-harmonic generation (SHG) is a powerful tool for probing the magnetic symmetries in  $\text{MPS}_3$  [18–22]. Using resonant SHG spectroscopy with symmetry analysis, we reveal possible two-peak features in the exciton-magnon spectra of  $\text{MnPS}_3$ , showing distinct anisotropies. This observation suggests the potential splitting of magnon bands caused by excitonic perturbations, as predicted by our Koster-Slater-type theory of magnons. Such exciton-magnon splitting, not observed in conventional 3D AFMs, underscores the presence of a substantial exciton-magnon interaction. Furthermore, a large magnetic-field-enhanced SHG at exciton resonance is revealed, attributed to an excitonic linear magnetoelectric effect. These findings provide renewed understandings on the correlation among quasiparticles in (quasi-)2D AFMs and may lead to the efficient and coherent generation of multi-mode magnons.

$\text{MnPS}_3$  has a monoclinic crystal structure with the space group  $C2/m$  [Fig. 1(a)] [10,23,24]. In the antiferromagnetic phase ( $T_N = 78$  K), the magnetic moments of  $\text{Mn}^{2+}$  ions ( $S = 5/2$ ) align at  $8^\circ$  to  $c^*$  in the  $ac$  plane ( $c^* \perp a, b$ ), with antiferromagnetic coupling between nearest neighbors, leading to the magnetic space group  $C2'/m$  [10,25]. The octahedral ( $O_h$ ) crystal field splits  $\text{Mn}^{2+} 3d^5$  high-spin state into multiple levels, including  ${}^6A_{1g}$ ,  ${}^4T_{1g}$ ,  ${}^4T_{2g}$ , and degenerate ( ${}^4E_g, {}^4A_{1g}$ ), among others, with observed exciton fine structures in the  ${}^6A_{1g} \rightarrow {}^4E_g, {}^4A_{1g}$  transition region, as shown in the absorption spectrum adapted from Ref. [17] [Fig. 1(b)]. In our experiments, the incident fundamental wavelength was adjusted to achieve resonance of the SH photon energy ( $2\hbar\omega$ )

\*These authors contributed equally to this work.

†Corresponding author: ziqian.wang@riken.jp

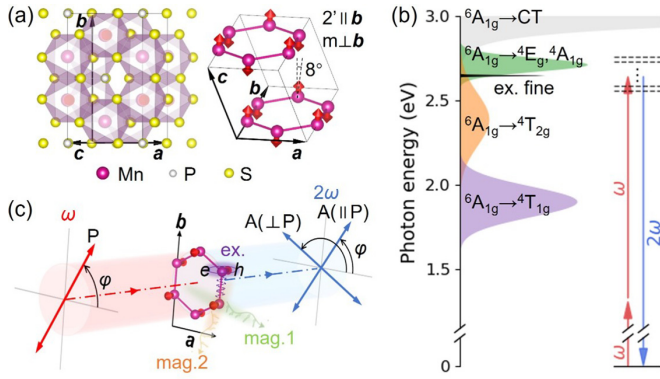


FIG. 1. Experimental setup for resonant SHG spectroscopy. (a) Crystal and magnetic structures of MnPS<sub>3</sub>. (b)  $d-d$  transitions and exciton fine structures shown with an absorption spectrum. SH photon energy was set to resonate with the exciton fine structures. (c) Transmission SHG geometry with fundamental and SH light paths normal to the  $ab$  plane. The optical excitation of excitons is expected to excite two types of magnons in exciton-magnon states.

with the fine structures [Fig. 1(b)], in order to reveal the symmetry/anisotropy of the excited states. A transmission geometry was employed, where the incident polarization ( $P$ ) and the generated SH polarization (through an analyzer,  $A$ ) are defined by the angle  $\varphi$  relative to the  $a$  axis [Fig. 1(c)].

Figure 2(a) shows the SHG spectra acquired by varying the incident wavelength from 920 to 950 nm (from 1.348 to 1.305 eV) with  $P \parallel A$ ,  $\varphi = 0^\circ$  at 3 K. No signal from these exciton fine structures was observed when they were off resonance, suggesting that the sharp peaks are purely from coherent SHG processes rather than incoherent ones such as two-photon luminescence. All the subsequent spectra were acquired at a 940 nm central wavelength as it finds strong resonances for the exciton and its sideband simultaneously. The polarization dependence of the SHG spectra for  $P \parallel A$  is shown in Fig. 2(b). A single-peaked exciton-resonant SHG with threefold symmetry is observed at 2.634 eV, denoted as  $E_0$ . In stark contrast, the sideband ranging from 2.638 to 2.648 eV comprises at least two subpeaks exhibiting distinct  $\varphi$  dependences. As detailed in Fig. 2(c), spectra at  $\varphi = 0^\circ$  and  $60^\circ$  reveal two major peaks in the sideband region, named  $EM_1$  and  $EM_2$ , centered at  $\sim 2.644$  and  $\sim 2.642$  eV, respectively, along with a minor peak  $E'$  at  $\sim 2.638$  eV and a weak broad background BG.

The temperature dependence of the fine structures helps to reveal their nature. Figure 2(d) shows the SHG spectra for  $P \parallel A$ ,  $\varphi = 0^\circ$  and  $60^\circ$  acquired at temperatures from 3 to 30 K. Peak  $E_0$  is only discernible below 20 K, while the sidebands survive up to 30 K. The peak positions for  $E_0$ ,  $EM_1$ ,  $EM_2$ , and  $E'$  are plotted against temperature in Fig. 2(e). In MnPS<sub>3</sub>, the magnon energy is known to decrease with increasing temperature due to the weakened exchange interaction [26], while the phonon energy remains mostly unchanged (less than 0.12 meV shift below 30 K [27]). Therefore, the obvious redshifts of  $EM_1$  and  $EM_2$  with increasing temperature reveal that they both have a magnon-sideband nature rather than a phonon sideband. Furthermore, the nearly constant energy and weak intensity of  $E'$  indicate that it is most likely a phonon sideband.

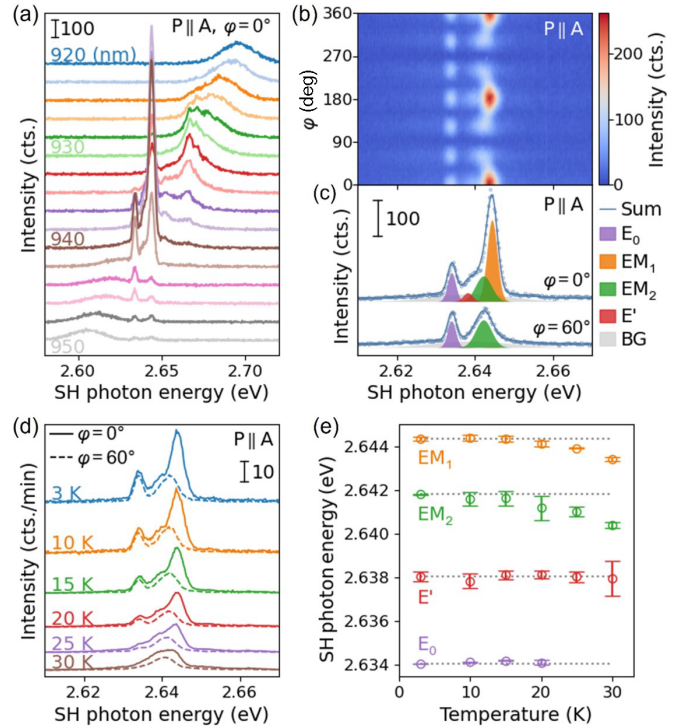


FIG. 2. Exciton fine structures in resonant SHG spectra. (a) Fundamental wavelength dependence of SHG spectra acquired at 2 nm intervals. 940 nm was chosen for the subsequent measurements. (b) Incident polarization ( $P$ ) dependence of SHG spectra with the analyzer ( $A$ ) set parallel to  $P$ . (c) SHG spectra at  $\varphi = 0^\circ$  and  $60^\circ$  with their components indicated. Four peaks  $E_0$ ,  $EM_1$ ,  $EM_2$ ,  $E'$  and one background BG were resolved. Spectra in (a)–(c) were acquired at 3 K. (d) Temperature dependence of SHG spectra at  $\varphi = 0^\circ$  and  $60^\circ$ . (e) Temperature dependence of  $E_0$ ,  $EM_1$ ,  $EM_2$ ,  $E'$  energy extracted from (d).

A bipartite AFM *without* intersublattice interactions holds sublattice exciton  $|E^i, \mathbf{k}\rangle$  or magnon  $|M^i, \mathbf{k}\rangle$  eigenstates residing on a single sublattice  $i$  ( $=a$  or  $b$ ) with wave vector  $\mathbf{k}$  [28,29]. The optically observable exciton line is  $|E^{a(b)}, \mathbf{0}\rangle$ , and the magnon sideband is an assembly of exciton-magnon states  $|E^{a(b)}, +\mathbf{k}; M^{b(a)}, -\mathbf{k}\rangle$  (and that with the sign of  $\mathbf{k}$  flipped) formed by an exciton and a magnon on different sublattices with opposite internal  $\mathbf{k}$ . For Mn<sup>2+</sup> ions whose  $d-d$  transitions involve a spin deviation [from  $S = 5/2$  to  $S = 3/2$ , Fig. 1(b)], sublattice excitons derived from single-ion excitations are parity and spin forbidden and only allowed by weak magnetic dipole (MD) transitions. In comparison, a compound exciton-magnon transition with canceled spin deviations on different sublattices is simultaneously spin and electric dipole (ED) allowed [30,31]. In real systems *with* intersublattice interactions, exciton or magnon wave functions can spread over neighboring sublattices, leading to the relaxation of parity/spin selection rules and the mixing of ED and MD characters. In MnPS<sub>3</sub>, an exciton-magnon transition is both ED and MD allowed for internal  $\mathbf{k}$  across the Brillouin zone (Supplemental Material Sec. I B [32]). Therefore, due to the near-flat exciton dispersion (Supplemental Material Sec. I C [32]) and assuming weak exciton-magnon interactions, the magnon sideband is anticipated to inherit mostly the

spectral features of magnon density of states (DOS) exhibiting a single peak (Fig. S3 [32]). The presence of two subpeaks  $EM_1$  and  $EM_2$  [Figs. 2(b) and 2(c)] thus strongly indicates a departure from the weak exciton-magnon interaction regime in MnPS<sub>3</sub>.

To gain insights into the symmetry of the fine structures, we present the rotational anisotropy (RA) of  $E_0$ ,  $EM_1$ , and  $EM_2$  intensities under different magnetic fields in Figs. 3(a) and 3(b) (see also Fig. S4 [32] for other magnetic field conditions). Notably,  $E_0$  demonstrates a substantial 70-fold enhancement under  $\pm 7$  T for both  $\mathbf{H} \parallel \mathbf{b}$  and  $\mathbf{H} \parallel \mathbf{a}$ . At  $H = 0$  [Figs. 3(a) and 3(b) middle left panels],  $E_0$  displays nearly isotropic

$$I_{\text{SH}} \propto \begin{cases} |(\chi_a \cos^2 \varphi + \chi_b \sin^2 \varphi + \chi_f \sin 2\varphi) \cos \varphi + (\chi_d \cos^2 \varphi + \chi_e \sin^2 \varphi - \chi_c \sin 2\varphi) \sin \varphi|^2, & P \parallel A, \\ |(\chi_a \cos^2 \varphi + \chi_b \sin^2 \varphi + \chi_f \sin 2\varphi) \sin \varphi - (\chi_d \cos^2 \varphi + \chi_e \sin^2 \varphi - \chi_c \sin 2\varphi) \cos \varphi|^2, & P \perp A. \end{cases} \quad (1)$$

Here,  $\chi_a = \chi_{111}^e + \chi_{211}^m$ ,  $\chi_b = \chi_{122}^e + \chi_{222}^m$ ,  $\chi_c = -\chi_{212}^e + \chi_{112}^m$ ,  $\chi_d = \chi_{211}^e - \chi_{111}^m$ ,  $\chi_e = \chi_{222}^e - \chi_{122}^m$ , and  $\chi_f = \chi_{112}^e + \chi_{212}^m$ , where  $\chi_{ijk}^e$  and  $\chi_{ijk}^m$  are the complex second-order nonlinear optical susceptibility tensors for ED and MD processes, respectively. Note that  $C2'/m$  (for  $H = 0$ ) and  $Cm$  (for  $\mathbf{H} \parallel \mathbf{b}$ ) require  $\chi_{d,e,f} = 0$ , leaving only  $\chi_{a,b,c}$  active, while  $C2'$  (for  $\mathbf{H} \parallel \mathbf{a}$ ) allows all  $\chi_{a,b,c,d,e,f}$  to be active. Detailed fitting results are provided in Supplemental Material Sec. I F [32], demonstrating smooth and systematic changes in  $\chi_{a,b,c,d,e,f}$  with  $|\mathbf{H}|$ . The presence of antiferromagnetic domains does not affect this analysis (Supplemental Material Sec. I F [32]).

The symmetric behavior of  $E_0$  with respect to sign reversal of  $H$  in Figs. 3(a) and 3(b) (left columns) is found to arise from the equal changes in  $\chi_{a,b}$  for  $\mathbf{H} \parallel \mathbf{b}$  and in  $\chi_{d,e}$  for  $\mathbf{H} \parallel \mathbf{a}$  (Fig. S5 [32]). This aligns well with the picture that the initially weak MD nature of zero-field  $E_0$  is swiftly overtaken by the strong ED component emerging under magnetic field, resulting in the substantial 70-fold enhancement at  $\pm 7$  T. Exemplary spectra of the significantly enhanced  $E_0$  peak in magnetic fields are shown in Fig. S7 [32]. Moreover, this magnetic-field-induced ED SH photon is polarized perpendicular to  $\mathbf{H}$  [Figs. 3(a) and 3(b) left columns], showing almost the same  $|\mathbf{H}|$  dependence for  $\mathbf{H} \parallel \mathbf{b}$  and  $\mathbf{H} \parallel \mathbf{a}$ . Such a near-isotropic field dependence of SHG efficiency again reflects the in-plane near-isotropic nature of  $E_0$  as observed in its zero-field SHG-RA patterns.

In stark contrast, both  $EM_1$  and  $EM_2$  respond asymmetrically to magnetic fields [Figs. 3(a) and 3(b) middle and right columns]. Under  $\mathbf{H} \parallel \mathbf{b}$ , the  $H$  asymmetry results from the prominent field dependencies of  $\chi_{a,b}$  for  $EM_1$  and  $EM_2$ , while for  $\mathbf{H} \parallel \mathbf{a}$ , the main contributors to the  $H$ -asymmetric pattern distortion of  $EM_1$  and  $EM_2$  are  $\chi_{d,e}$  (Fig. S5 [32]). The coupling between magnetic field  $\mathbf{H} \parallel \mathbf{b}$  ( $\mathbf{H} \parallel \mathbf{a}$ ) and  $\chi_{a,b}$  ( $\chi_{d,e}$ ) can be explained by their similar transformation properties, or the same irreducible corepresentations (ICRs), derived from group theory (Supplemental Material Sec. I D [32]). The asymmetric magnetic field dependences suggest the interference between ED and MD processes of similar magnitudes in both  $EM_1$  and  $EM_2$ , consistent with the earlier description of their characteristics based on group theoretical considerations (Supplemental Material Sec. I B [32]). Intriguingly, a closer

threefold patterns, despite the broken threefold symmetry of the magnetic space group  $C2'/m$ . This near-isotropic threefold symmetry is consistent with the local  $O_h$  crystal field of Mn<sup>2+</sup>, thereby indicating the highly localized nature of the pure exciton  $E_0$ . In contrast, both  $EM_1$  and  $EM_2$  present highly anisotropic twofold patterns at  $H = 0$ , which is distinct from the threefold local symmetry but well in line with the global  $C2'/m$  symmetry of a monolayer/bulk, suggesting the wave or extended nature of  $EM_1$  and  $EM_2$ .

The SHG-RA patterns in Figs. 3(a) and 3(b) are further analyzed with the symmetry-adapted SH intensity formula.

examination of the fitting parameters reveals that the relation Eq. (2) is constantly satisfied in the complex numbers  $\chi_{a,b,c,d,e,f}$  for  $EM_1$  and  $EM_2$  under all magnetic field conditions, and this is more evident in the circular polarization

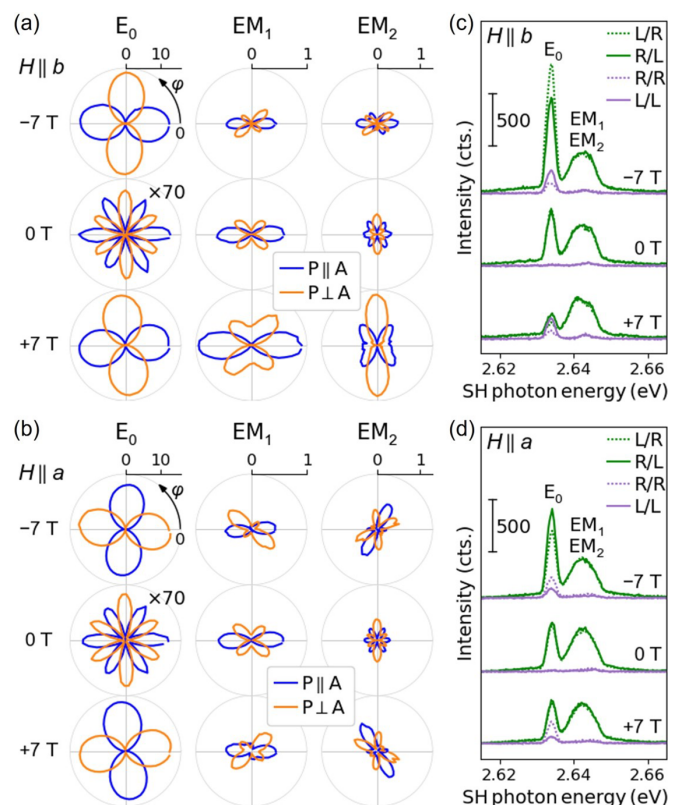


FIG. 3. Light polarization and magnetic field dependence of  $E_0$ ,  $EM_1$  and  $EM_2$ . (a), (b) Linear polarization SHG-RA patterns of  $E_0$ ,  $EM_1$ , and  $EM_2$  under  $\mathbf{H}$  along the  $b$  and  $a$  axes. Patterns in each column have a common scale bar. (c), (d) Circular polarization SHG spectra under  $\mathbf{H}$  along the  $b$  and  $a$  axes. L(R)/L(R): Circular polarizations of fundamental/SH photons. All measurements were carried out at 3 K.

SHG spectra as in the following,

$$\chi_a - \chi_b \approx 2\chi_c, \quad \chi_d - \chi_e \approx 2\chi_f. \quad (2)$$

This relation serves as an informative clue for our symmetry analysis of the exciton-magnon states.

Figures 3(c) and 3(d) show the circular polarization SHG spectra under magnetic fields (see also Fig. S6 [32] for other magnetic field conditions). The SH intensities in these cases are given below:

$$I_{\text{SH}} \propto \begin{cases} |(\chi_a - \chi_b - 2\chi_c) - i(\chi_d - \chi_e - 2\chi_f)|^2, & L/L, \\ |(\chi_a - \chi_b - 2\chi_c) + i(\chi_d - \chi_e - 2\chi_f)|^2, & R/R, \\ |(\chi_a - \chi_b + 2\chi_c) + i(\chi_d - \chi_e + 2\chi_f)|^2, & L/R, \\ |(\chi_a - \chi_b + 2\chi_c) - i(\chi_d - \chi_e + 2\chi_f)|^2, & R/L. \end{cases} \quad (3)$$

Here,  $L(R)/L(R)$  denotes the left-handed (right-handed) circular polarization for fundamental/SH light. Again,  $\chi_{d,e,f} = 0$  holds for both  $H = 0$  ( $C2'/m$ ) and  $\mathbf{H} \parallel \mathbf{b}$  ( $Cm$ ). Remarkably, for  $EM_1$  and  $EM_2$  (2.638–2.648 eV),  $L/R$  and  $R/L$  overlap and show almost no magnetic field dependence, and  $L/L$  and  $R/R$  signals are constantly zero. This observation confirms that Eq. (2) holds individually for  $EM_1$  and  $EM_2$ . In contrast,  $E_0$  shows different peak intensities for the four polarization configurations at finite magnetic fields and exhibits distinct field dependences, thereby indicating the breakdown of Eq. (2) for the pure exciton (Supplemental Material Sec. I G [32]). It is noteworthy that the magnetic space groups  $C2'/m$ ,  $Cm$ , and  $C2'$  impose no other constraints on the relation among  $\chi_{a,b,c,d,e,f}$  than the vanishing of  $\chi_{d,e,f}$  as  $H$  approaches 0. Equation (2) thus reflects the higher symmetry of the states in  $EM_1$  and  $EM_2$ , which arises from the presence of equally weighted  $\Gamma_1$  and  $\Gamma_2$  ICR characteristics in each exciton-magnon state (Supplemental Material Sec. I D [32]).

The overall similarities between  $EM_1$  and  $EM_2$  revealed by SHG suggest that they should bear similar and related physical origins, e.g., exciton-magnon states split from the same source. To explain this behavior, we developed a Koster-Slater-type theory for magnons on a Néel AFM honeycomb lattice under the local influence due to a Frenkel exciton (see Supplemental Material Sec. II [32] for detailed formulations). For concreteness, we conceive a physical picture of an exciton localized around an atomic site as the disturbance to the spin Hamiltonian, which changes local spin magnitude (from  $5/2$  to  $3/2$ ) and exchange interaction (from  $J$  to  $J + \delta J$ ) in its vicinity [Fig. 4(a)]. The spin Hamiltonian  $\mathcal{H} = 2 \sum_{\langle l,m \rangle} J_{lm} \mathbf{S}_l \cdot \mathbf{S}_m$  only includes nearest neighbors due to their dominant contribution [42].

By solving the Green's function for the local cluster directly influenced by the exciton, two types of magnon sidebands appear. To see this, the spectral function  $\text{tr}[A(\omega)]$  with the sublattices summed up for the two sidebands are shown in Fig. 4(b) with varying  $\delta J$  values. The spectrum nearly invariant with  $\delta J$  (green) corresponds to a quasifree magnon band, while the other with a significant  $\delta J$  dependence (orange) corresponds to a quasibound one as the resonance occurs at an energy with finite DOS. The quasibound curve originates from the unit cell containing the localized exciton, while the quasifree one arises from the unit cell nearby (see

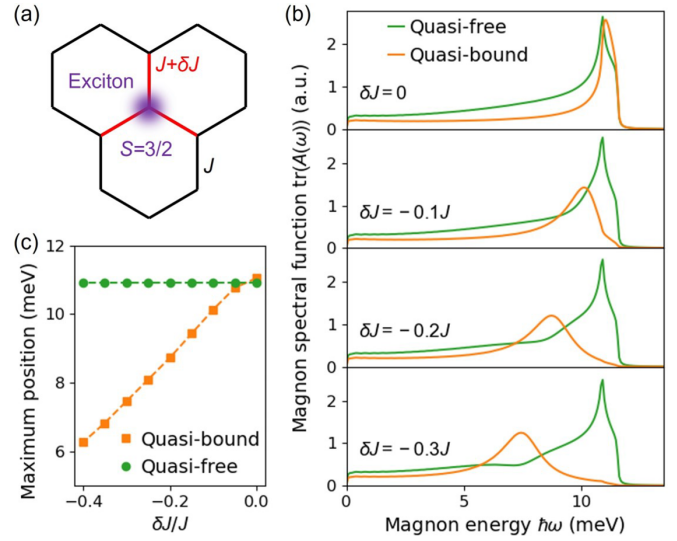


FIG. 4. Theoretical calculation showing exciton-induced magnon splitting in  $\text{MnPS}_3$ . (a) A localized exciton perturbs the spin magnitude ( $S$ ) and exchange interaction ( $J$ ). (b) Calculated magnon spectral function with varying  $\delta J$ . The quasifree band shows little variation, while the quasibound band exhibits a significant shift and typically a broader profile. (c)  $\delta J$  dependence of the energy at the maximum points of the two bands. Agreement between the  $EM_1/EM_2$  in the SHG spectra [Fig. 2(c)] and the quasifree/quasibound bands in the calculation at  $\delta J \sim -0.25J$  can be observed.

Supplemental Material Sec. II B [32] for details). In particular, the narrower-dispersion quasifree band has a peak position that matches the energy of  $EM_1$  relative to  $E_0$ , while the quasibound band has a similar broadened feature as  $EM_2$ . This correlation suggests a correspondence between the theoretically predicted quasifree and quasibound bands and the magnon components of the experimentally observed  $EM_1$  and  $EM_2$ , respectively.

As is clear from Figs. 4(b) and 4(c),  $\delta J$  is decisive to the splitting magnitude between the quasifree and quasibound magnons. The generation of a Frenkel exciton from the  $\text{Mn}^{2+}$  high-spin ground state with half-filled  $d$  orbitals will create unoccupied and double-occupied orbitals, which allow ferromagnetic exchange processes with neighbors according to Goodenough-Kanamori-Anderson rules, thereby reducing the antiferromagnetic coupling in its vicinity and leading to negative  $\delta J$ . A comparison between the theoretical spectral functions and the SHG spectra implies a  $\sim 25\%$  reduction of local exchange interaction caused by an exciton. In addition, the exciton-induced magnon splitting in  $\text{MnPS}_3$ , not identified in 3D AFMs, suggests a much stronger charge-spin-orbital correlation in this (quasi-)2D AFM.

From a symmetry perspective, the large exciton-magnon splitting in  $\text{MnPS}_3$  is associated with the shared transformation properties (ICRs) of excitons and magnons for all internal  $\mathbf{k}$ , fully unlocking their interactions, enabled by the material's specific site and global symmetry. This contrasts with the typical 3D AFM  $\text{MnF}_2$ , where exciton-magnon interactions are much suppressed due to the lack of mutual ICRs in excitons and magnons at the majority high-symmetry points.

A full group theoretical discussion on the magnon splitting and the related symmetry aspects of the exciton-magnon SHG is provided in Supplemental Material Secs. I B and I D [32].

Furthermore, as illustrated by the cartoon view in Fig. 1(c), an exciton, efficiently generated by an incident photon, simultaneously excites a magnon from either of the two magnon branches by conserving the momentum, and may lead to ultrafast multimode magnon control.

In addition, the nearly equal enhancement of  $E_0$  SHG efficiency under two orthogonal  $\mathbf{H}$  directions [Figs. 3(a) and 3(b) left columns] is a probe for the ED-SHG-active static electric polarization  $P_y$  ( $P_x$ ) of the exciton, induced by the static magnetic field  $H_x$  ( $H_y$ ). The rotation of the exciton-originated transition dipole with  $\mathbf{H}$  is in agreement with the linear magnetoelectric effect, denoted as  $P_i = \alpha_{ij}H_j$ , with  $i, j = x, y$  and  $\alpha_{xy}, \alpha_{yx} \neq 0$ ,  $\alpha_{xx} = \alpha_{yy} = 0$  for  $C2'/m$  [10],

thereby demonstrating the linear magnetoelectric effect of the exciton.

We thank Dr. Y. Murakami, Dr. J. J. He, Dr. Y. Liu, and Dr. J. Lehmann for valuable discussions. Z.W. was supported by JSPS KAKENHI Grant No. 21K13889 and RIKEN Incentive Research Projects. X.-X.Z. was partially supported by RIKEN Special Postdoctoral Researcher Program. Y.S. was supported by JSPS KAKENHI Grant No. 22H05449. N.N. and Y.T. were supported by CREST-JST (JPMJCR1874). N.N. was supported also by JSPS KAKENHI Grant No. 18H03676. N.O. was supported by JSPS KAKENHI Grant No. 22H01185.

Z.W. and N.O. designed the project and performed the SHG experiments and symmetry analysis; X.-X.Z. and N.N. performed the theoretical calculation and analysis; Y.S. grew the bulk single crystal; all authors collaborated in interpreting the data.

- 
- [1] K. F. Mak, J. Shan, and D. C. Ralph, Probing and controlling magnetic states in 2D layered magnetic materials, *Nat. Rev. Phys.* **1**, 646 (2019).
- [2] G. Long, H. Henck, M. Gibertini, D. Dumcenco, Z. Wang, T. Taniguchi, K. Watanabe, E. Giannini, and A. F. Morpurgo, Persistence of magnetism in atomically thin MnPS<sub>3</sub> crystals, *Nano Lett.* **20**, 2452 (2020).
- [3] S. Y. Kim, T. Y. Kim, L. J. Sandilands, S. Sinn, M. C. Lee, J. Son, S. Lee, K. Y. Choi, W. Kim, B. G. Park, C. Jeon, H. D. Kim, C. H. Park, J. G. Park, S. J. Moon, and T. W. Noh, Charge-spin correlation in van der Waals antiferromagnet NiPS<sub>3</sub>, *Phys. Rev. Lett.* **120**, 136402 (2018).
- [4] S. Kang, K. Kim, B. H. Kim, J. Kim, K. I. Sim, J.-U. Lee, S. Lee, K. Park, S. Yun, T. Kim, A. Nag, A. Walters, M. Garcia-Fernandez, J. Li, L. Chapon, K.-J. Zhou, Y.-W. Son, J. H. Kim, H. Cheong, and J.-G. Park, Coherent many-body exciton in van der Waals antiferromagnet NiPS<sub>3</sub>, *Nature (London)* **583**, 785 (2020).
- [5] W. Xing, L. Qiu, X. Wang, Y. Yao, Y. Ma, R. Cai, S. Jia, X. C. Xie, and W. Han, Magnon transport in quasi-two-dimensional van der Waals antiferromagnets, *Phys. Rev. X* **9**, 011026 (2019).
- [6] R. Cheng, S. Okamoto, and D. Xiao, Spin Nernst effect of magnons in collinear antiferromagnets, *Phys. Rev. Lett.* **117**, 217202 (2016).
- [7] Y. Shiomi, R. Takashima, and E. Saitoh, Experimental evidence consistent with a magnon Nernst effect in the antiferromagnetic insulator MnPS<sub>3</sub>, *Phys. Rev. B* **96**, 134425 (2017).
- [8] R. Takashima, Y. Shiomi, and Y. Motome, Nonreciprocal spin Seebeck effect in antiferromagnets, *Phys. Rev. B* **98**, 020401(R) (2018).
- [9] E. V. Boström, T. S. Parvini, J. W. McIver, A. Rubio, S. V. Kusminskiy, and M. A. Sentef, All-optical generation of antiferromagnetic magnon currents via the magnon circular photogalvanic effect, *Phys. Rev. B* **104**, L100404 (2021).
- [10] E. Ressouche, M. Loire, V. Simonet, R. Ballou, A. Stunault, and A. Wildes, Magnetoelectric MnPS<sub>3</sub> as a candidate for ferrotoroidicity, *Phys. Rev. B* **82**, 100408(R) (2010).
- [11] M. Matthiesen, J. R. Hortensius, S. Mañas-Valero, I. Kapon, D. Dumcenco, E. Giannini, M. Šiškins, B. A. Ivanov, H. S. J. van der Zant, E. Coronado, A. B. Kuzmenko, D. Afanasiev, and A. D. Caviglia, Controlling magnetism with light in a zero orbital angular momentum antiferromagnet, *Phys. Rev. Lett.* **130**, 076702 (2023).
- [12] C. A. Belvin, E. Baldini, I. O. Ozel, D. Mao, H. C. Po, C. J. Allington, S. Son, B. H. Kim, J. Kim, I. Hwang, J. H. Kim, J.-G. Park, T. Senthil, and N. Gedik, Exciton-driven antiferromagnetic metal in a correlated van der Waals insulator, *Nat. Commun.* **12**, 4837 (2021).
- [13] D. Afanasiev, J. R. Hortensius, M. Matthiesen, S. Mañas-Valero, M. Šiškins, M. Lee, E. Lesne, H. S. J. van der Zant, P. G. Steeneken, B. A. Ivanov, E. Coronado, and A. D. Caviglia, Controlling the anisotropy of a van der Waals antiferromagnet with light, *Sci. Adv.* **7**, eabf3096 (2021).
- [14] K. Hwangbo, Q. Zhang, Q. Jiang, Y. Wang, J. Fonseca, C. Wang, G. M. Diederich, D. R. Gamelin, D. Xiao, J.-H. Chu, W. Yao, and X. Xu, Highly anisotropic excitons and multiple phonon bound states in a van der Waals antiferromagnetic insulator, *Nat. Nanotechnol.* **16**, 655 (2021).
- [15] X. Wang, J. Cao, Z. Lu, A. Cohen, H. Kitadai, T. Li, Q. Tan, M. Wilson, C. H. Lui, D. Smirnov, S. Sharifzadeh, and X. Ling, Spin-induced linear polarization of photoluminescence in antiferromagnetic van der Waals crystals, *Nat. Mater.* **20**, 964 (2021).
- [16] E. Ergeçen, B. Ilyas, D. Mao, H. C. Po, M. B. Yilmaz, J. Kim, J.-G. Park, T. Senthil, and N. Gedik, Magnetically brightened dark electron-phonon bound states in a van der Waals antiferromagnet, *Nat. Commun.* **13**, 98 (2022).
- [17] S. L. Gnatchenko, I. S. Kachur, V. G. Piryatinskaya, Y. M. Vysochanskii, and M. I. Gurzan, Exciton-magnon structure of the optical absorption spectrum of antiferromagnetic MnPS<sub>3</sub>, *Low Temp. Phys.* **37**, 144 (2011).
- [18] H. Chu, C. J. Roh, J. O. Island, C. Li, S. Lee, J. Chen, J. G. Park, A. F. Young, J. S. Lee, and D. Hsieh, Linear magnetoelectric phase in ultrathin MnPS<sub>3</sub> probed by optical second harmonic generation, *Phys. Rev. Lett.* **124**, 027601 (2020).
- [19] Z. Ni, A. V. Haglund, H. Wang, B. Xu, C. Bernhard, D. G. Mandrus, X. Qian, E. J. Mele, C. L. Kane, and L. Wu, Imaging the Néel vector switching in the monolayer antiferromagnet

- MnPS<sub>3</sub> with strain-controlled Ising order, *Nat. Nanotechnol.* **16**, 782 (2021).
- [20] Z. Ni, H. Zhang, D. A. Hopper, A. V. Haglund, N. Huang, D. Jariwala, L. C. Bassett, D. G. Mandrus, E. J. Mele, C. L. Kane, and L. Wu, Direct imaging of antiferromagnetic domains and anomalous layer-dependent mirror symmetry breaking in atomically thin MnPS<sub>3</sub>, *Phys. Rev. Lett.* **127**, 187201 (2021).
- [21] Z. Ni, N. Huang, A. V. Haglund, D. G. Mandrus, and L. Wu, Observation of giant surface second-harmonic generation coupled to nematic orders in the van der Waals antiferromagnet FePS<sub>3</sub>, *Nano Lett.* **22**, 3283 (2022).
- [22] J.-Y. Shan, M. Ye, H. Chu, S. Lee, J.-G. Park, L. Balents, and D. Hsieh, Giant modulation of optical nonlinearity by Floquet engineering, *Nature (London)* **600**, 235 (2021).
- [23] A. R. Wildes, H. M. Rønnow, B. Roessli, M. J. Harris, and K. W. Godfrey, Static and dynamic critical properties of the quasi-two-dimensional antiferromagnet MnPS<sub>3</sub>, *Phys. Rev. B* **74**, 094422 (2006).
- [24] K. Momma and F. Izumi, VESTA3 for three-dimensional visualization of crystal, volumetric and morphology data, *J. Appl. Crystallogr.* **44**, 1272 (2011).
- [25] T. Hicks, T. Keller, and A. Wildes, Magnetic dipole splitting of magnon bands in a two dimensional antiferromagnet, *J. Magn. Mater.* **474**, 512 (2019).
- [26] O. Nagai and T. Tanaka, Temperature-dependent magnon-energy theory of FeF<sub>2</sub> and MnF<sub>2</sub>, *Phys. Rev.* **188**, 821 (1969).
- [27] Y.-J. Sun, Q.-H. Tan, X.-L. Liu, Y.-F. Gao, and J. Zhang, Probing the magnetic ordering of antiferromagnetic MnPS<sub>3</sub> by Raman spectroscopy, *J. Phys. Chem. Lett.* **10**, 3087 (2019).
- [28] D. D. Sell, R. L. Greene, and R. M. White, Optical exciton-magnon absorption in MnF<sub>2</sub>, *Phys. Rev.* **158**, 489 (1967).
- [29] D. D. Sell, Review of magnon-sideband experiments, *J. Appl. Phys.* **39**, 1030 (1968).
- [30] R. Loudon, Theory of infra-red and optical spectra of antiferromagnets, *Adv. Phys.* **17**, 243 (1968).
- [31] Y. Tanabe, T. Moriya, and S. Sugano, Magnon-induced electric dipole transition moment, *Phys. Rev. Lett.* **15**, 1023 (1965).
- [32] See Supplemental Material at <http://link.aps.org/supplemental/10.1103/PhysRevResearch.5.L042032> for materials and methods, group theoretical analyses, additional discussion on linear and circular polarization SHG results, and details of theoretical calculations, which includes Refs. [33–41].
- [33] J. C. Diels and W. Rudolph, *Ultrashort Laser Pulse Phenomena*, 2nd ed. (Academic Press/Elsevier, Amsterdam, 2006).
- [34] Y. Xu, L. Elcoro, Z.-D. Song, B. J. Wieder, M. G. Vergniory, N. Regnault, Y. Chen, C. Felser, and B. A. Bernevig, High-throughput calculations of magnetic topological materials, *Nature (London)* **586**, 702 (2020).
- [35] L. Elcoro, B. J. Wieder, Z. Song, Y. Xu, B. Bradlyn, and B. A. Bernevig, Magnetic topological quantum chemistry, *Nat. Commun.* **12**, 5965 (2021).
- [36] C. J. Bradley and B. L. Davies, Magnetic groups and their corepresentations, *Rev. Mod. Phys.* **40**, 359 (1968).
- [37] M. Lax and J. J. Hopfield, Selection rules connecting different points in the Brillouin zone, *Phys. Rev.* **124**, 115 (1961).
- [38] A. Missetich and R. E. Dietz, Role of exciton dispersion and exciton-magnon interactions on the shape of magnon sidebands in stressed MnF<sub>2</sub>, *J. Appl. Phys.* **39**, 1145 (1968).
- [39] A. R. Wildes, S. Okamoto, and D. Xiao, Search for nonreciprocal magnons in MnPS<sub>3</sub>, *Phys. Rev. B* **103**, 024424 (2021).
- [40] A. L. Kuzemsky, *Statistical Mechanics and the Physics of Many-Particle Model Systems* (World Scientific, Singapore, 2016).
- [41] S. T. Pantelides, The electronic structure of impurities and other point defects in semiconductors, *Rev. Mod. Phys.* **50**, 797 (1978).
- [42] A. R. Wildes, B. Roessli, B. Lebech, and K. W. Godfrey, Spin waves and the critical behaviour of the magnetization in MnPS<sub>3</sub>, *J. Phys.: Condens. Matter* **10**, 6417 (1998).